Microscopic origin of anomalous interlayer exciton transport in van der Waals heterostructures

Daniel Erkensten [1], Samuel Brem [2], Raül Perea-Causín [1], and Ermin Malic [2,1]

[1]*Department of Physics, Chalmers University of Technology, 41296 Gothenburg, Sweden*
[2]*Department of Physics, Philipps-Universität Marburg, 35037 Marburg, Germany*

Van der Waals heterostructures constitute a platform for investigating intriguing many-body quantum phenomena. In particular, transition-metal dichalcogenide (TMD) heterobilayers host long-lived interlayer excitons which exhibit permanent out-of-plane dipole moments. Here, we develop a microscopic theory for interlayer exciton-exciton interactions including both the dipolar nature of interlayer excitons as well as their fermionic substructure, which gives rise to an attractive fermionic exchange. We find that these interactions contribute to a drift force resulting in highly nonlinear exciton propagation at elevated densities in the $MoSe_2 - WSe_2$ heterostructure. We show that the propagation can be tuned by changing the number of hBN spacers between the TMD layers or by adjusting the dielectric environment. In particular, although counterintuitive, we reveal that interlayer excitons in freestanding samples propagate slower than excitons in hBN-encapsulated TMDs—due to an enhancement of the net Coulomb drift with stronger environmental screening. Overall, our work contributes to a better microscopic understanding of the interlayer exciton transport in technologically promising atomically thin semiconductors.

I. INTRODUCTION

In recent years, van der Waals heterostructures have emerged as a new class of 2D materials providing a promising playground for studying strong correlations and exotic phases of matter [1–4]. These structures may be formed by stacking transition-metal dichalcogenide (TMD) monolayers on top of each other, which enables the formation of long-lived interlayer excitons [5–8], i.e., Coulomb-bound electron-hole pairs where the electronic constituents reside in different layers; cf. Fig. 1. Due to the large separation between electrons and holes, interlayer excitons exhibit permanent out-of-plane dipole moments. These result in strong repulsive inter-excitonic interactions, which are of crucial importance for many-body phenomena in the quantum regime [9–12].

In particular, the effect of strong dipole repulsion has been observed in photoluminescence measurements [10,13], where the interaction becomes manifest in density-dependent blueshifts of the emission energy with increasing pump power. Moreover, recent experimental studies [10,12] display the crucial impact of repulsive exciton-exciton interactions in interlayer exciton propagation and transport at elevated electron-hole densities. In this context, highly nonlinear exciton diffusion was observed and attributed to the net drift

flux of interlayer excitons caused by the repulsive interactions. However, despite the first experiments displaying the importance of the interlayer exciton-exciton interaction in van der Waals heterostructures, its microscopic origin and the role of the exchange coupling and excitonic screening have remained elusive. Furthermore, strategies on how to experimentally control the Coulomb-induced exciton drift have not been systematically studied so far.

In this work, we present a microscopic theory of exciton-exciton interactions and study their impact on interlayer exciton propagation in the exemplary $MoSe_2 - WSe_2$ heterostructure. While most previous studies have focused on dipole-dipole repulsion explaining the nonlinear exciton diffusion [12–14], we show that it is of crucial importance to also consider the fermionic exchange interactions [15–17] and excitonic screening [18,19]; cf. Fig. 1. We reveal that the interplay of these partially counteracting mechanisms determines the overall spatiotemporal dynamics of interlayer excitons. In particular, we find that the repulsive interlayer exciton-exciton interaction is considerably reduced by the attractive exchange interaction. These interactions generate a net drift force which leads to an increase in the effective diffusion coefficient by up to an order of magnitude at high exciton densities, resulting in a highly nonlinear interlayer exciton propagation. Moreover, we find that the latter can be tuned by changing the interlayer distance, e.g., through the inclusion of hBN spacers (Fig. 1), thereby enhancing the repulsive dipolar interactions between interlayer excitons. Finally, we predict a counterintuitive dependence on the dielectric environment, where freestanding heterostructures exhibit a smaller exciton drift, despite the stronger Coulomb interaction between individual charges in a purely classical picture.
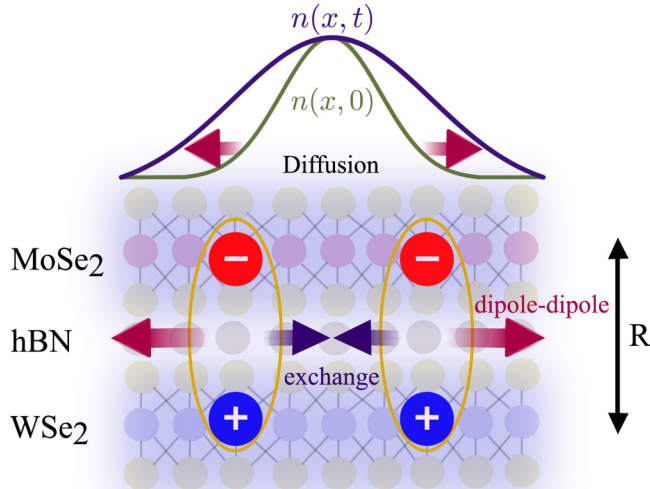
FIG. 1. Schematic illustration of the repulsive dipole-dipole interaction (red arrows) and attractive exchange interaction (blue arrows) between interlayer excitons in the exemplary $MoSe_2 - WSe_2$ heterostructure. Dipole-dipole repulsion plays a crucial role at elevated densities and leads to a strong drift of the interlayer exciton distribution $n(x, t)$.

II. THEORETICAL MODEL

To describe intra- and interlayer exciton-exciton interactions in a microscopic and material-specific way we combine the exciton density matrix formalism [20–22] with density functional theory calculations [23]. First, we derive the mean-field Hamilton operator $H = H_0 + H_{x-x}$, consisting of the free part (H_0) and the inter-excitonic interaction part (H_{x-x}). We express the Hamiltonian in an excitonic basis with $H_0 = \sum_{\alpha, \boldsymbol{Q}} E^{\alpha}_{\boldsymbol{Q}} X^{\dagger}_{\alpha, \boldsymbol{Q}} X_{\alpha, \boldsymbol{Q}}$ and

$$H_{x-x} = \sum_{\substack{\alpha, \beta \\ \boldsymbol{Q}, \boldsymbol{q}}} W^{\alpha\beta}_{\mathrm{mf}, \boldsymbol{q}, \boldsymbol{Q}} X^{\dagger}_{\alpha, \boldsymbol{Q}-\boldsymbol{q}} X_{\beta, \boldsymbol{Q}}. \qquad (1)$$

Here, $X^{(\dagger)}_{\alpha, \boldsymbol{Q}}$ are excitonic operators creating or annihilating an exciton in the state $\alpha = 1s, 2p, 2s, \dots$ with the center-of-mass momentum $\boldsymbol{Q}$. The exciton dispersion $E^{\alpha}_{\boldsymbol{Q}} = \frac{\hbar^2 \boldsymbol{Q}^2}{2M} + E^{\alpha}$ includes the exciton binding energy E^{α}, which is obtained along with the associated excitonic wave functions $\varphi_{\alpha, \boldsymbol{q}}$ by solving the Wannier equation [24]. The appearing exciton mass M is obtained from DFT calculations [23]. The full derivation of the mean-field Hamiltonian and the used DFT parameters can be found in the Supplemental Material [25].

The interaction term, H_{x-x}, contains the mean-field exciton-exciton matrix element, $W^{\alpha\beta}_{\mathrm{mf}, \boldsymbol{q}, \boldsymbol{Q}}$, which includes direct and exchange contributions. In general, both contributions are momentum-dependent, but the matrix element for $1s$ excitons is approximately constant in the long-wavelength limit and reads

$$\lim_{\boldsymbol{q}, \boldsymbol{Q} \to 0} W^{1s-1s}_{\mathrm{mf}, \boldsymbol{q}, \boldsymbol{Q}} = n_x (g_{d-d} + g_{x-x}). \qquad (2)$$

The full expression for the momentum-dependent matrix element is given in the Supplemental Material. Note that the full momentum-dependent matrix elements have been investigated in detail in a previous study [21]. In this work

we consider low temperatures and cold exciton distributions peaked around $\boldsymbol{Q} = 0$, and therefore restrict our studies to the long-wavelength approximation of the exciton-exciton interaction. In the context of interlayer exciton transport, the long-wavelength approximation holds as the length scale of the exciton spatial profile ($\sim \mu$m) is much larger than the length scale of the exciton-exciton interaction ($\sim$ nm); cf. the Supplemental Material. Moreover, we consider interactions between the mostly occupied $1s$ exciton states, neglecting the coupling to higher-order exciton states. We have introduced the exciton density n_x and the dipole-dipole interaction strength g_{d-d}, which reads

$$g^{(X)}_{d-d} = 0, \quad g^{(IX)}_{d-d} = \frac{e^2}{2\epsilon_0} \left(\frac{d_1}{\epsilon^{(1)}_{\perp}} + \frac{d_2}{\epsilon^{(2)}_{\perp}} + \frac{2R}{\epsilon_R} \right) \qquad (3)$$

for intralayer (X) and interlayer (IX) excitons. Here, e is the electron charge, d_i the TMD layer thickness, $\epsilon^{(i)}_{\perp}$ the out-of-plane component of the dielectric tensor [26] of the TMD layer $i = 1, 2$, R the layer separation, and ϵ_R the effective dielectric constant for a spacer with the thickness R; cf. Fig. 1. While the dipole-dipole interaction between ground state intralayer excitons vanishes, for interlayer excitons we find a considerable repulsive (>0) interaction that can be interpreted as a classical dipole-dipole coupling [21,27].

Since excitons are composite bosons consisting of electrons and holes, exchange of fermionic constituents [16,22] also has to be included when considering exciton-exciton interactions. In contrast to the classical dipole-dipole coupling, the exchange interaction strength depends strongly on the excitonic wave functions and reads

$$g_{x-x} = A \sum_{\boldsymbol{k}, \boldsymbol{k}'} |\varphi_{\boldsymbol{k}'}|^2 \left(2 V^{eh}_{\boldsymbol{k}} \varphi^*_{\boldsymbol{k}+\boldsymbol{k}'} \varphi_{\boldsymbol{k}'} - \sum_{\lambda=e,h} V^{\lambda\lambda}_{\boldsymbol{k}} |\varphi_{\boldsymbol{k}'+\boldsymbol{k}}|^2 \right), \quad (4)$$

where A is the crystal area. Note that the appearing electronic Coulomb matrix elements $V^{\lambda\lambda}_{\boldsymbol{k}}$ and $V^{\lambda\bar{\lambda}}_{\boldsymbol{k}}$ ($\lambda \neq \bar{\lambda}$) are proportional to $1/A$, such that g_{x-x} is independent of A. The first term in Eq. (4) is proportional to the electron-hole interaction ($V^{eh}_{\boldsymbol{k}}$), while the second is determined by the electron-electron ($V^{ee}_{\boldsymbol{k}}$) and hole-hole ($V^{hh}_{\boldsymbol{k}}$) interactions [16,28]. Importantly, the contributions V^{eh} and V^{ee}/V^{hh} come with different signs, reflecting the attractive and repulsive nature of the electron-hole and electron-electron (hole-hole) coupling, respectively.

The nature of the exchange part of the exciton-exciton interaction between intralayer and interlayer excitons is fundamentally different. In particular, it holds that $V^{eh}_{\boldsymbol{k}} \approx V^{hh}_{\boldsymbol{k}} \approx V^{ee}_{\boldsymbol{k}}$ ($V^{eh}_{\boldsymbol{k}} \ll V^{ee}_{\boldsymbol{k}}, V^{hh}_{\boldsymbol{k}}$) for interactions between intralayer (interlayer) excitons; i.e., the electron-hole interaction is significantly weaker than the Coulomb repulsion between individual electrons or holes when electrons and holes are spatially separated in different layers. As a consequence, the exchange interaction becomes more attractive (negative) as the vertical separation of electrons and holes is increased [29]. In contrast, the exchange interaction between intralayer excitons is always repulsive (positive) [30].

When evaluating the electronic Coulomb matrix elements ($V^{eh}_{\boldsymbol{k}}, V^{ee}_{\boldsymbol{k}}, V^{hh}_{\boldsymbol{k}}$) we take into account (i) the finite thickness of the TMD sample and the dielectric screening due to the surrounding substrate and the TMD monolayers themselves, and (ii) the excitonic screening present at elevated

electron-hole densities. The first (background) contribution is obtained as a generalized Rytova-Keldysh potential [6,31,32] and the latter is calculated using static excitonic polarizabilities via an excitonic Lindhard model [18,19], inducing a density dependence in the exciton-exciton interaction (see Supplemental Material for more details). Note, however, that the exciton wave functions are still taken as density-independent, which is assumed to hold as long as the exciton-exciton interaction energy is smaller than the binding energy and can be seen as a perturbative correction to the exciton energy. This assumption is justified in this work as we consider densities at which most electron-hole pairs are bound as excitons, i.e., densities below the exciton Mott transition at $\sim 10^{13}$ cm^{-2} [19]. The negligence of free carrier screening allows us to obtain a theory expressed entirely in excitonic quantities. Note that although excitons (being effectively neutral quasiparticles) are only weakly polarizable compared to the free plasma, we find that the inclusion of higher-lying p states, e.g., $1s - 2p$ exciton transitions, gives rise to a significant screening stemming from bound states [19] (cf. the Supplemental Material). Finally, we point out that the mean-field treatment of excitons introduced here, considering excitons as pure and independent bosons with the fermionic exchange effects captured via the excitonic Coulomb matrix elements, neglects the formation of biexcitons or higher-order particle clusters. Moreover, the theory is expected to hold up to first order in exciton density, n_x. In particular, this translates to fulfilling the condition $n_x a_B^2 \ll 1$, corresponding to exciton densities $n_x \ll 10^{14}$ cm^{-2} assuming an exciton Bohr radius $a_B \sim 1$ nm [27].

III. DENSITY-DEPENDENT SPECTRAL SHIFTS

We now make use of the Hamiltonian in (1) to determine the density-dependent spectral shifts of exciton resonances, which are accessible, e.g., in photoluminescence spectra [10,13]. These shifts can be microscopically calculated directly from the equation of motion for the bright exciton polarization, $P_{1s} = \langle X_{1s,\boldsymbol{Q}=0}^\dagger \rangle$, which on a Hartree-Fock level reads (cf. the Supplemental Material)

$$\dot{P}_{1s} = \frac{i}{\hbar}(E^{1s} + \Delta E(n_x))P_{1s} \tag{5}$$

with $n_x = \frac{1}{A}\sum_{\boldsymbol{Q}}\langle X_{\boldsymbol{Q}}^\dagger X_{\boldsymbol{Q}}\rangle$. Here, we introduced the density-dependent energy renormalization

$$\Delta E(n_x) \equiv (g_{d-d} + g_{x-x})n_x + \Sigma_{CH}. \tag{6}$$

The last term describes the Coulomb-hole contribution [33], which explicitly takes into account density-dependent screening effects of the electronic band gap. It reads $\Sigma_{CH} = \sum_{\boldsymbol{q}}(V_{\boldsymbol{q}}^{hh} - \bar{V}_{\boldsymbol{q}}^{hh})$, where $\bar{V}_{\boldsymbol{q}}^{hh}$ denotes the *unscreened* Coulomb potential with respect to exciton screening. Hence, within our formalism, the Coulomb-hole term describes the reduction of the exciton energy due to a screening-induced change in the Coulomb renormalization of the filled valence band (cf. the Supplemental Material for details).

In Fig. 2 we present the corresponding density-dependent energy renormalization for interlayer [Fig. 2(a)] and intralayer excitons [Fig. 2(b)] in the exemplary MoSe$_2$ − WSe$_2$ heterobilayer and WSe$_2$ monolayer, respectively. Due to the

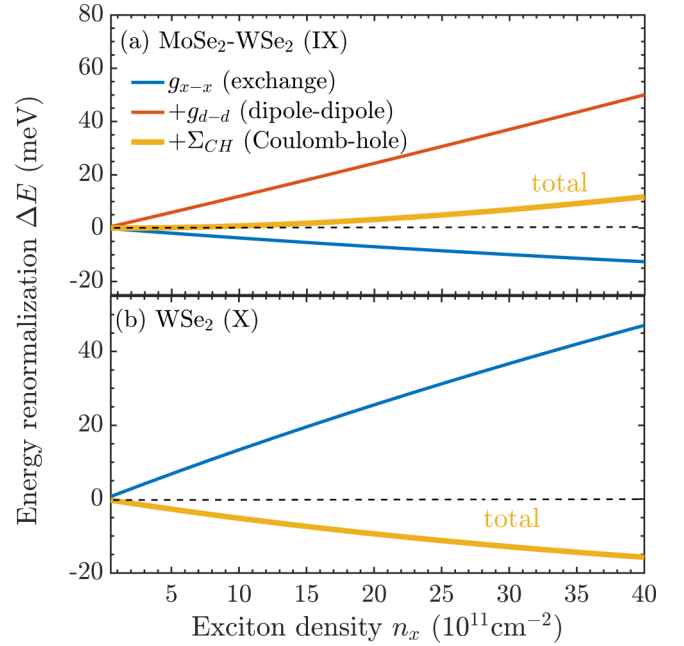FIG. 2. Density-dependent energy renormalization ΔE due to the exchange interaction (g_{x-x}; blue), the dipole-dipole interaction (g_{d-d}; red), and the screening-induced Coulomb-hole contribution (yellow). Note that the individual contributions are included additively. (a) Interlayer energy renormalization in the MoSe$_2$ − WSe$_2$ heterostructure, resulting in a net blueshift of the exciton resonance. (b) Intralayer energy renormalization in the WSe$_2$ monolayer, resulting in a net redshift.

strong dipole-dipole interaction (g_{d-d}) in the heterostructure we obtain a net blueshift—in agreement with experimental studies [12,13,34]. In contrast, a small redshift is found in the intralayer case due to the absence of permanent dipole moments. Here, we note that the intralayer exciton-exciton interaction is dominated by quantum-mechanical exchange interactions (g_{x-x}), as has been confirmed previously for TMD monolayers [21,35] and quantum wells [15,27,30]. Moreover, as discussed above, the exchange interaction is repulsive (attractive) in the intralayer (interlayer) case. The nature of this interaction depends strongly on the interplay between the electron-hole and electron-electron/hole-hole Coulomb matrix element; cf. Eq. (4). By including the screening between excitons at elevated densities, the blueshift of the interlayer exciton resonance is reduced, resulting in a net shift on the order of 15 meV for the considered density range ($0 \leqslant n_x < 5 \times 10^{12}$ cm^{-2}).

Finally, we also observe the predominant role of the Coulomb-hole term in monolayers, compensating for the exchange-induced shift to higher energies and even leading to a net redshift of intralayer exciton resonances—in agreement with experimental observations [10] and previous microscopic calculations [36]. Note that correlation effects and free carrier screening are neglected here, which could reduce the shift of exciton resonances further.

In the following, we will focus on spatially inhomogeneous systems, assuming density gradients on much larger scales than the exciton Bohr radius/thermal wave length. In real space, the energy shifts discussed above translate into

a spatially varying potential $\Delta E(n(x, y))$ which leads to a drift of excitons. Thus, we now consider the propagation of interlayer excitons and focus in particular on the impact of exciton-exciton interactions.

IV. COULOMB-DRIVEN EXCITON PROPAGATION

The spatiotemporal dynamics of excitons can be accessed through the temporal evolution of the exciton Wigner function [37–39], which is directly extracted from the Heisenberg equation of motion for the off-diagonal density matrix $\langle X_Q^\dagger X_{Q'} \rangle$. Extending the approach introduced by Hess and Kuhn [40,41] to excitons, we can quantitatively describe the spatiotemporal evolution of the interlayer exciton density $n(\mathbf{r}, t)$ through the following drift-diffusion equation:

$$\dot{n}(\mathbf{r}, t) = \nabla \cdot [D(n(\mathbf{r}, t))\nabla n(\mathbf{r}, t)]$$

$$+ \mu_m \nabla \cdot [\Delta E(n(\mathbf{r}, t))\nabla n(\mathbf{r}, t)] - \frac{n(\mathbf{r}, t)}{\tau}, \quad (7)$$

with $D(n) = D_0 \frac{T_d}{T}[\exp(T_d/T) - 1]^{-1}$, where D_0 is the low-density diffusion coefficient, $T_d = \frac{2\pi n \hbar^2}{M k_B}$ the degeneracy temperature, $\mu_m = \frac{D_0}{k_B T}$ the exciton mobility, and τ the exciton lifetime [42]. At the cryogenic temperatures ($T \ll T_d$) considered in this work, the diffusion coefficient D acquires a strong density dependence as a result of boson bunching. Here, we have included the spatially varying exciton-exciton interaction energy $\Delta E(n(\mathbf{r}, t))$ [Eq. (6)] consisting of contributions from the dipole-dipole interaction (g_{d-d}), the exchange interactions (g_{x-x}), and the Coulomb-hole term (Σ_{CH}). Note that we disregard exciton-exciton annihilation processes [43,44] in this work. These are assumed to be negligible for interlayer excitons, as has been confirmed by recent time-dependent photoluminescence measurements in $MoSe_2 - WSe_2$ [12] as well as $WS_2 - WSe_2$ heterobilayers [10]. Additional details on the derivation of (7) are found in the Supplemental Material.

The first term in Eq. (7) accounts for the diffusive propagation of excitons and leads to conventional diffusion at low excitation densities with a time-independent propagation speed given by the low-density diffusion coefficient D_0 according to Fick's law [37,45]. The second term, which arises due to net repulsive exciton-exciton interactions, leads to a drift flux of interlayer excitons and is therefore denoted as the Coulomb-induced drift. Finally, the third term in (7) describes the population decay of the interlayer exciton density. By numerically solving the drift-diffusion equation [Eq. (7)] for an exemplary hBN-encapsulated $MoSe_2$-hBN-WSe_2 heterostructure (Fig. 1), we gain microscopic access to the spatiotemporal dynamics of interlayer excitons. In the considered AA-stacked heterostructure we note that the bright KK interlayer exciton state is by far the energetically lowest state due to the large type-II band alignment [46], and therefore it is justified to restrict our analysis to this state. Moreover, we can neglect the effects of hybridization due to the weak interlayer tunneling strength at the K point [47,48]. The inclusion of an hBN spacer with the thickness $R = 0.3$ nm additionally allows us to disregard the possibility of interlayer excitons being trapped by the moiré potential, which is known to affect exciton transport in van der Waals heterostructures [3,49,50].

Furthermore, we adapt our study to the experimental conditions of Ref. [12] by setting the temperature to $T = 4.6$ K, the low-density diffusion coefficient $D_0 = 0.15$ cm^2/s, and the exciton lifetime $\tau = 3.5$ ns obtained from transport measurements. In Fig. 3(a) we illustrate the exciton density $n(x, y, t)$ for different times t. We initialize the exciton distribution as a Gaussian, $n(x, y, 0) = n_x \exp[-(x^2 + y^2)/\sigma_0^2]$, and specify the initial density $n_x = 5 \times 10^{12}$ cm^{-2} and laser spot size $\sigma_0^2 = 1$ μm^2. As time progresses, the density develops into a super-Gaussian distribution whose spatial width, given by $\sigma_t^2 = \int \mathbf{r}^2 n(\mathbf{r}, t)d\mathbf{r} / \int n(\mathbf{r}, t)d\mathbf{r}$, evolves highly nonlinearly with time—a hallmark of *anomalous* diffusion; cf. Fig. 3(c).

Including just the diffusive part of the exciton transport [$\propto D$; cf. Eq. (7)], the exciton distribution retains its Gaussian shape; cf. Fig. 3(b). However, as the diffusion coefficient decreases rapidly with density at low temperatures (due to boson bunching), the width of the exciton distribution varies sublinearly with time [blue, solid lines in Fig. 3(c)]. It stays approximately constant when comparing with the case of a constant diffusion coefficient D_0, in which the width increases linearly with time, i.e., $\sigma_t^2 - \sigma_0^2 = 4D_0 t$, according to Fick's law [blue, dashed lines in Fig. 3(c)]. Instead, the transport properties of interlayer excitons are governed by exciton-exciton interactions at elevated densities. In particular, the repulsive dipole-dipole interaction leads to the drift of interlayer excitons giving rise to a fast propagation, which is much enhanced relative to diffusion. In particular, we obtain an effective diffusion coefficient of $D_{\text{eff}} = 1.5$ cm^2/s from the slope of the variance (at $t = 1.5$ ns), which is one order of magnitude larger than the low density diffusion coefficient of $D_0 = 0.15$ cm^2/s. The net impact of the interaction is reduced when also taking into account the exchange interaction—reflecting its attractive nature [cf. Eq. (4)]—and the Coulomb-hole contribution [cf. Eq. (6)]. The latter significantly reduces the interaction potential at elevated densities, as observed in Fig. 3(c), and weakens the Coulomb-induced drift due to dipole-dipole interaction; cf. solid purple lines. For comparison, we provide the time-dependent variance as obtained from solving the drift-diffusion equation assuming a constant diffusion coefficient D_0; cf. the dashed purple lines. This corresponds to assuming a Boltzmann distribution for excitons, retrieved by taking the classical limit $T \gg T_d$ in Eq. (7). As exciton drift completely dominates over diffusion at elevated densities and the exciton mobility is only dependent on the low-density diffusion coefficient, it follows that the solid and dashed lines qualitatively coincide and that the anomalous character of the transport is only weakly dependent on the exciton distribution.

As a consequence of the interplay between the repulsive (dipole-dipole) and attractive (exchange and Coulomb-hole) contributions to the Coulomb-induced drift, considerably high densities are needed to actually observe an anomalous exciton diffusion. The density dependence of the interlayer exciton transport is investigated further in Fig. 3(d), where we find that densities larger than $n_x = 10^{12}$ cm^{-2} are required to observe nonlinear exciton propagation. At densities $n_x \leqslant 10^{12}$ cm^{-2} the propagation becomes purely diffusive and exciton-exciton interactions play a minor role. In particular, at densities $n_x = 10^{12}$ cm^{-2} (green curve) and below, the time-dependent
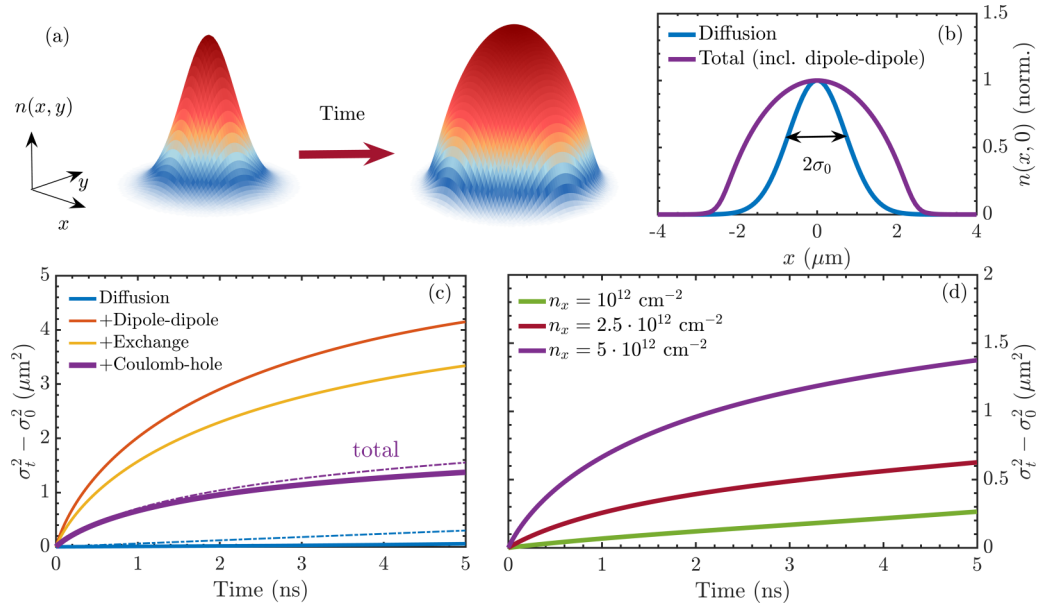
FIG. 3. Time evolution of interlayer exciton density $n(x, y, t)$ in the $MoSe_2$-hBN-WSe_2 heterostructure at 4.6 K. (a) Exciton distribution initialized as a Gaussian distribution with an initial variance set to $\sigma_0^2 = 1\ \mu m^2$ and an exciton density of $n_x = 5 \times 10^{12}\ cm^{-2}$. As time progresses a significant broadening of the distribution is observed due to the strong repulsive exciton-exciton interaction. (b) Cut of the exciton distribution $n(x, 0)$ at $t = 5$ ns with (purple) and without (blue) the Coulomb-induced drift. (c) Time-dependent variances σ_t^2 at the exciton density $n_x = 5 \times 10^{12}\ cm^{-2}$ taking into account just conventional diffusion (blue) and including Coulomb drift stemming from the exchange interaction, the dipole-dipole repulsion, and the Coulomb-hole term. The dashed lines show the solution of the drift-diffusion equation assuming a Boltzmann distribution for the interlayer exciton including only diffusion (blue) and including both diffusion and Coulomb-induced drift terms (purple). (d) Impact of the exciton density on the interlayer exciton transport. Anomalous diffusion is observed at densities $n_x > 10^{12}\ cm^{-2}$.

variance $\sigma_t^2 - \sigma_0^2$ approaches $4D_0t$ with the low-density diffusion coefficient D_0, as expected from Fick's law.

V. TUNABILITY OF THE COULOMB-INDUCED INTERLAYER EXCITON DRIFT

Having determined the microscopic nature of exciton-exciton interactions in van der Waals heterostructures and their impact on exciton propagation, we now investigate how the propagation can be tuned. The possibility to control the exciton transport is of technological relevance for the design of devices based on atomically thin semiconductors. In particular, successful control of exciton transport paves the way for creating excitonic devices, such as transistors [51]. In the following, we identify and investigate three experimentally accessible knobs to tune the propagation of excitons: (i) interlayer distance, (ii) dielectric environment, and (iii) excitation spot size.

Interlayer distance. The dipole-dipole interaction between interlayer excitons is highly tunable with the layer separation, R (cf. Fig. 1), as observed in recent experimental studies [10,12]. In particular, we find that the dipole moment of interlayer excitons is enhanced by more than 50% by including an hBN spacer into the heterostructure. As a direct consequence, the dipole-dipole interaction [Eq. (3)] can be boosted by increasing the layer separation. Here, we show how a change of the interlayer separation affects the Coulomb-induced drift on microscopic footing, including the impact on the exchange interaction as well as exciton screening.

In Fig. 4, we show the time-dependent effective diffusion coefficients $D_{eff}(t) \equiv \frac{1}{4}\frac{d}{dt}\sigma_t^2$ for an increasing number of hBN spacers. We find that interlayer excitons propagate
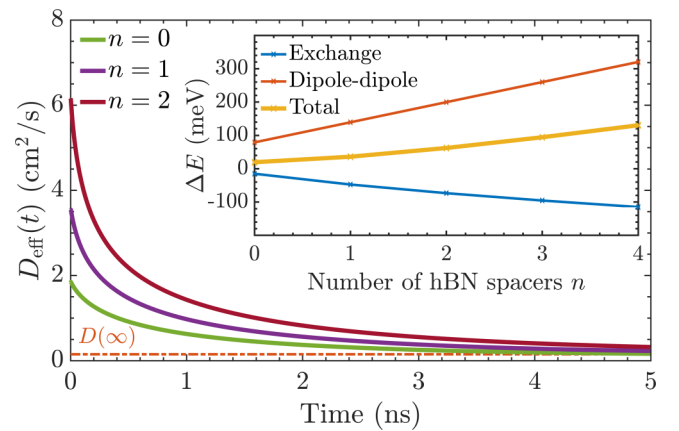

FIG. 4. Time-dependent effective diffusion coefficient $D_{eff}(t) \equiv \frac{1}{4}\frac{d}{dt}\sigma_t^2$ for different numbers of hBN spacers placed between the two layers in the $MoSe_2 - WSe_2$ heterostructure for a fixed exciton density $n_x = 5 \times 10^{12}\ cm^{-2}$. A drastic increase in the diffusion coefficient at initial times is found with the number of hBN spacers. At large times ($t \to \infty$) the coefficients approach the indicated low-density coefficient $D = 0.15\ cm^2/s$ (dashed orange line). The inset illustrates the dependence of the exciton-exciton interaction energy ΔE [cf. Eq. (6)] on the layer separation and shows that the total interaction (yellow line) is boosted with an increasing number of hBN spacers.

faster when the interlayer separation is larger. This reflects the increased contribution of the dipole-dipole repulsion, as shown in the inset in Fig. 4. Note that the exchange interaction is also very sensitive to changes in the interlayer distance— as it crucially depends on the electron-hole interaction—and it partially counteracts the classical dipole-dipole repulsion (cf. inset). In particular, we find that the reduction of the electron-hole interaction with interlayer distance results in a decrease in the exciton binding energy from ≈ 90 meV to ≈ 78 meV when comparing hBN-encapsulated $MoSe_2 - WSe_2$ heterostructures with and without a hBN spacer, respectively, indicating that the exciton stays tightly bound in the presence of a small number of spacers. Importantly, the Coulomb-induced drift of excitons gives rise to a significant enhancement of the effective diffusion coefficient at initial times, when the exciton density is at its largest. The diffusion coefficients range from $D_{eff} \approx 6$ cm^2/s to $D_{eff} \approx 2$ cm^2/s when considering heterostructures with and without hBN spacers, respectively. This corresponds to an enhancement of more than an order of magnitude compared to the low-density diffusion coefficient of $D = 0.15$ cm^2/s (indicated by the dashed line in Fig. 4). At larger times, the exciton density drops as excitons have propagated away from the excitation spot, leading to the low-density regime where the impact of exciton-exciton interaction is small and conventional diffusion is predominant.

Dielectric engineering. Besides varying the number of hBN spacers between the TMD monolayers, the exciton-exciton interaction can be tuned by changing the surrounding environment, i.e., by modifying the dielectric constant of the surrounding material, ϵ_s. We find that the dipole repulsion and the exchange coupling exhibit only a weak dependence on the dielectric environment. Figure 5(a) illustrates the changes in the energy renormalization ΔE [Eq. (6)] as a function of the dielectric constant. In the considered long-wavelength limit, the dipole-dipole interaction is independent of screening [cf. Eq. (3)] and the exchange interaction [cf. Eq. (4)] leads to a very small change in ΔE (in the range of just a few meV from the freestanding to the hBN-encapsulated samples). This is in stark contrast to the conventional Coulomb interaction between electrons and holes, in which the Coulomb matrix elements are approximately inversely proportional to ϵ_s. In general, the exciton-exciton interaction is determined by the Coulomb potentials V^{eh}, V^{ee}, and V^{hh}, but it additionally depends on form factors that scale with the excitonic wave functions in momentum space $\sim |\varphi_k|^4$ [cf. Eq. (4)]. As the dielectric constant of the environment is increased, the Coulomb interaction is weakened, which makes the excitonic wave function less localized in real space. This means, however, that the wave function becomes narrower in momentum space resulting in larger form factors. Visually speaking, when the Bohr radius of the exciton is increased it is more likely that two excitons occupy the same space, which increases the interaction strength. The competition between increased exciton wave function overlap and weakened Coulomb interactions is the microscopic origin of the observed weak screening dependence of g_{d-d} and g_{x-x}; cf. Fig. 5(a).

While the dielectric properties of the environment do not significantly impact the strength of the dipole-dipole and exchange interactions, we find that the nonlinear time
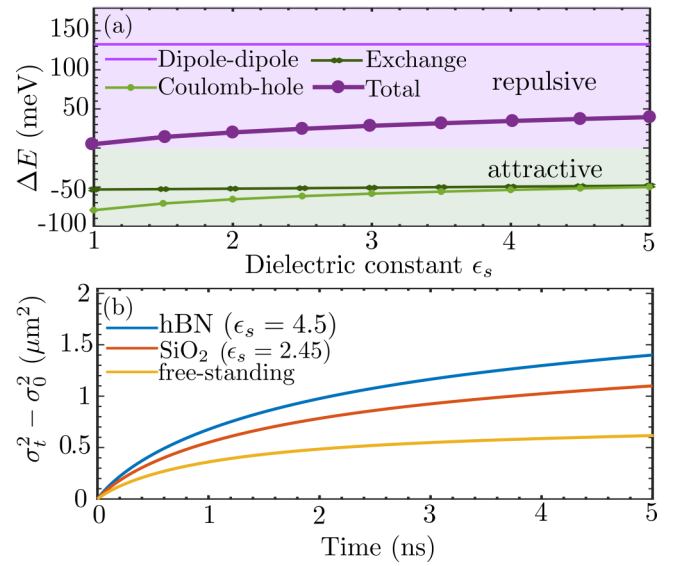

FIG. 5. Impact of dielectric environment on spectral shift and transport of interlayer excitons at a fixed exciton density $n_x = 5 \times 10^{12}$ cm^{-2}. (a) Screening dependence of the energy renormalization ΔE distinguishing different contributions. The total exciton-exciton interaction (purple line) shows only a weak dependence that can be traced back to the Coulomb-hole contribution (bright green line). (b) Temporal evolution of the variance $\sigma_t^2 - \sigma_0^2$ as a function of time for different surrounding substrates.

dependence of the variance σ_t^2 can still be strongly tuned with dielectric engineering. As we show in Fig. 5(b), hBN-encapsulated samples are seen to result in more anomalous (faster) diffusion than freestanding TMDs. This is a counterintuitive result, as one would expect the Coulomb-induced drift to be more efficient in the freestanding case, where the screening of the Coulomb interaction is weak. We can trace back this striking behavior to the screening dependence of the Coulomb-hole term [Eq. (6)]; cf. the bright green line in Fig. 5(a). In particular, we find that this term can be expressed through the exciton polarizability Π_q according to $\Sigma_{CH} = -\sum_q \frac{(V_q^{hh})^2 |\Pi_q|}{1 + V_q^{hh} |\Pi_q|}$, where Π_q approximately scales with the ratio of the in-plane exciton transition dipole moment and the $1s - 2p$ transition energy (cf. the Supplemental Material). When the dielectric constant ϵ_s is increased, the exciton Bohr radius—and therefore the $1s - 2p$ transition dipole—is enhanced, and at the same time the $1s - 2p$ transition energy is reduced [7], thus boosting the polarizability. However, the weakening of the Coulomb potential V_q^{hh} with increasing dielectric constant dominates over the enhancement of the polarizability. This results in a less attractive (negative) Coulomb-hole interaction for high dielectric constants. As a consequence, the Coulomb-hole term counteracts the dominating repulsive dipole-dipole interactions more strongly for freestanding TMD heterostructures.

Excitation spot size. Here, we study the impact of the laser spot size on the interlayer exciton transport. By initializing the exciton density as $n(x, y, 0) = \frac{N_x}{\pi \sigma_0^2} \exp[-(x^2 + y^2)/\sigma_0^2]$ and keeping the total number of excitons, N_x, constant (i.e., considering a constant laser pump power), we investigate the
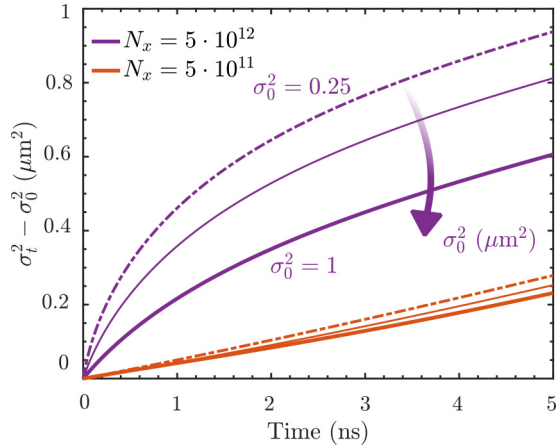
FIG. 6. Impact of initial laser spot size on interlayer exciton transport. The exciton density is initialized as $n(x, y, 0) = \frac{N_x}{\pi \sigma_0^2} \exp[-(x^2 + y^2)/\sigma_0^2]$ such that the total number of excitons N_x is kept constant when varying the spot size, σ_0^2. For two different N_x, we study different spot sizes $\sigma_0^2 = 0.25, 0.5,$ and 1 (in units of μm^2). Increasing the spot size effectively results in a smaller initial exciton density, making exciton-exciton interaction less important and anomalous exciton diffusion less enhanced.

change in the variance for different initial laser spots with $\sigma_0^2 = 0.25, 0.5, 1$ μm^2; cf. Fig. 6. For a relatively low number of excitons, $N_x = 5 \times 10^{11}$ (orange lines), we find that the Coulomb-induced drift is less important and conventional diffusion dominates the exciton transport. As expected from Fick's law of conventional diffusion, the choice of σ_0^2 is not expected to significantly affect the propagation. However, as we increase the number of excitons N_x to $N_x = 5 \times 10^{12}$ (purple lines), we observe a much more pronounced effect of the initial spot size. We find a decrease in the effective diffusion

coefficient from $D_{\text{eff}}(t_0) \approx 1 \text{ cm}^2/\text{s}$ to $D_{\text{eff}}(t_0) \approx 0.5 \text{ cm}^2/\text{s}$ at $t_0 = 0.5$ ns when increasing the spot size from $\sigma_0^2 = 0.25$ μm^2 to $\sigma_0^2 = 1$ μm^2. This can be explained by the fact that increasing the spot size effectively reduces the initial exciton density at the center of the excitation spot.

VI. CONCLUSIONS

We have investigated the impact of exciton-exciton interaction on the propagation of excitons in the exemplary $MoSe_2 - WSe_2$ heterostructure. We find that there is a competition between the repulsive dipole-dipole coupling with exchange interaction and exciton screening. The interplay of these processes gives rise to a net Coulomb-induced drift that accelerates the propagation of interlayer excitons at elevated densities. Furthermore, we demonstrate how this Coulomb-induced drift and the resulting anomalous exciton propagation can be tuned by changing the interlayer separation (e.g., varying the number of hBN spacers), dielectric environment, or laser spot size. The developed approach could be generalized to include also the hybridization between intra- and interlayer excitons allowing for the investigation of exciton-exciton interactions in any van der Waals heterostructure. Overall, our work contributes to a better microscopic understanding of interlayer exciton transport in technologically promising atomically thin semiconductors.

[1] Y. Liu, N. O. Weiss, X. Duan, H.-C. Cheng, Y. Huang, and X. Duan, Nat. Rev. Mater. **1**, 16042 (2016).

[2] K. Novoselov, A. Mishchenko, A. Carvalho, and A. M. Castro Neto, Science **353**, aac9439 (2016).

[3] S. Brem, C. Linderälv, P. Erhart, and E. Malic, Nano Lett. **20**, 8534 (2020).

[4] S. Brem and E. Malic, Nano Lett. **22**, 1311 (2022).

[5] P. Rivera, J. R. Schaibley, A. M. Jones, J. S. Ross, S. Wu, G. Aivazian, P. Klement, K. Seyler, G. Clark, N. J. Ghimire *et al.*, Nat. Commun. **6**, 6242 (2015).

[6] S. Ovesen, S. Brem, C. Linderälv, M. Kuisma, T. Korn, P. Erhart, M. Selig, and E. Malic, Commun. Phys. **2**, 23 (2019).

[7] P. Merkl, F. Mooshammer, P. Steinleitner, A. Girnghuber, K.-Q. Lin, P. Nagler, J. Holler, C. Schüller, J. M. Lupton, T. Korn *et al.*, Nat. Mater. **18**, 691 (2019).

[8] N. Peimyoo, T. Deilmann, F. Withers, J. Escolar, D. Nutting, T. Taniguchi, K. Watanabe, A. Taghizadeh, M. F. Craciun, K. S. Thygesen *et al.*, Nat. Nanotechnol. **16**, 888 (2021).

[9] Z. Wang, D. A. Rhodes, K. Watanabe, T. Taniguchi, J. C. Hone, J. Shan, and K. F. Mak, Nature (London) **574**, 76 (2019).

[10] L. Yuan, B. Zheng, J. Kunstmann, T. Brumme, A. B. Kuc, C. Ma, S. Deng, D. Blach, A. Pan, and L. Huang, Nat. Mater. **19**, 617 (2020).

[11] I. V. Bondarev, O. L. Berman, R. Y. Kezerashvili, and Y. E. Lozovik, Commun. Phys. **4**, 134 (2021).

[12] Z. Sun, A. Ciarrocchi, F. Tagarelli, J. F. Gonzalez Marin, K. Watanabe, T. Taniguchi, and A. Kis, Nat. Photonics **16**, 79 (2022).

[13] P. Nagler, G. Plechinger, M. V. Ballottin, A. Mitioglu, S. Meier, N. Paradiso, C. Strunk, A. Chernikov, P. C. Christianen, C. Schüller *et al.*, 2D Mater. **4**, 025112 (2017).

[14] V. Shahnazaryan and H. Rostami, Phys. Rev. B **104**, 085405 (2021).

[15] C. Schindler and R. Zimmermann, Phys. Rev. B **78**, 045313 (2008).

[16] F. Tassone and Y. Yamamoto, Phys. Rev. B **59**, 10830 (1999).

[17] P. Rivera, K. L. Seyler, H. Yu, J. R. Schaibley, J. Yan, D. G. Mandrus, W. Yao, and X. Xu, Science **351**, 688 (2016).

[18] G. Röpke and R. Der, Phys. Status Solidi B **92**, 501 (1979).

[19] A. Steinhoff, M. Florian, M. Rösner, G. Schönhoff, T. O. Wehling, and F. Jahnke, Nat. Commun. **8**, 1166 (2017).

[20] S. Brem, A. Ekman, D. Christiansen, F. Katsch, M. Selig, C. Robert, X. Marie, B. Urbaszek, A. Knorr, and E. Malic, Nano Lett. **20**, 2849 (2020).

[21] D. Erkensten, S. Brem, and E. Malic, Phys. Rev. B **103**, 045426 (2021).

[22] F. Katsch, M. Selig, A. Carmele, and A. Knorr, Phys. Status Solidi B **255**, 1800185 (2018).

[23] A. Kormányos, G. Burkard, M. Gmitra, J. Fabian, V. Zólyomi, N. D. Drummond, and V. Fal'ko, 2D Mater. **2**, 022001 (2015).

[24] M. Kira and S. W. Koch, Prog. Quantum Electron. **30**, 155 (2006).

[25] See Supplemental Material at http://link.aps.org/supplemental/10.1103/PhysRevMaterials.6.094006 for additional details on the derivation of the interlayer exciton-exciton interaction, the drift-diffusion equation for excitons, and input parameters; also see Refs. [52–60] therein.

[26] A. Laturia, M. L. Van de Put, and W. G. Vandenberghe, npj 2D Mater. Appl. **2**, 6 (2018).

[27] S. B.-T. de-Leon and B. Laikhtman, Phys. Rev. B **63**, 125306 (2001).

[28] A. Bobrysheva, M. Miglei, and M. Shmiglyuk, Phys. Status Solidi B **53**, 71 (1972).

[29] O. Kyriienko, E. B. Magnusson, and I. A. Shelykh, Phys. Rev. B **86**, 115324 (2012).

[30] C. Ciuti, V. Savona, C. Piermarocchi, A. Quattropani, and P. Schwendimann, Phys. Rev. B **58**, 7926 (1998).

[31] N. S Rytova, Proc. MSU, Phys. Astron. **3**, 30 (1967).

[32] L. V. Keldysh, Sov. Phys. JETP **29**, 658 (1979).

[33] L. Hedin, Phys. Rev. **139**, A796 (1965).

[34] W. Li, X. Lu, S. Dubey, L. Devenica, and A. Srivastava, Nat. Mater. **19**, 624 (2020).

[35] V. Shahnazaryan, I. Iorsh, I. A. Shelykh, and O. Kyriienko, Phys. Rev. B **96**, 115409 (2017).

[36] D. Erben, A. Steinhoff, C. Gies, G. Schönhoff, T. O. Wehling, and F. Jahnke, Phys. Rev. B **98**, 035434 (2018).

[37] R. Perea-Causín, S. Brem, R. Rosati, R. Jago, M. Kulig, J. D. Ziegler, J. Zipfel, A. Chernikov, and E. Malic, Nano Lett. **19**, 7317 (2019).

[38] R. Rosati, R. Schmidt, S. Brem, R. Perea-Causín, I. Niehues, J. Kern, J. A. Preuß, R. Schneider, S. Michaelis de Vasconcellos, R. Bratschitsch *et al.*, Nat. Commun. **12**, 7221 (2021).

[39] R. Rosati, R. Perea-Causín, S. Brem, and E. Malic, Nanoscale **12**, 356 (2020).

[40] O. Hess and T. Kuhn, Phys. Rev. A **54**, 3347 (1996).

[41] O. Hess and T. Kuhn, Prog. Quantum Electron. **20**, 85 (1996).

[42] A. Ivanov, Europhys. Lett. **59**, 586 (2002).

[43] Y. Yu, Y. Yu, C. Xu, A. Barrette, K. Gundogdu, and L. Cao, Phys. Rev. B **93**, 201111(R) (2016).

[44] D. Erkensten, S. Brem, K. Wagner, R. Gillen, R. Perea-Causín, J. D. Ziegler, T. Taniguchi, K. Watanabe, J. Maultzsch, A. Chernikov *et al.*, Phys. Rev. B **104**, L241406 (2021).

[45] M. Kulig, J. Zipfel, P. Nagler, S. Blanter, C. Schüller, T. Korn, N. Paradiso, M. M. Glazov, and A. Chernikov, Phys. Rev. Lett. **120**, 207401 (2018).

[46] R. Gillen and J. Maultzsch, Phys. Rev. B **97**, 165306 (2018).

[47] Y. Wang, Z. Wang, W. Yao, G.-B. Liu, and H. Yu, Phys. Rev. B **95**, 115429 (2017).

[48] J. Hagel, S. Brem, C. Linderälv, P. Erhart, and E. Malic, Phys. Rev. Research **3**, 043217 (2021).

[49] J. Choi, W.-T. Hsu, L.-S. Lu, L. Sun, H.-Y. Cheng, M.-H. Lee, J. Quan, K. Tran, C.-Y. Wang, M. Staab *et al.*, Sci. Adv. **6**, eaba8866 (2020).

[50] J. Wang, Q. Shi, E.-M. Shih, L. Zhou, W. Wu, Y. Bai, D. Rhodes, K. Barmak, J. Hone, C. R. Dean, and X.-Y. Zhu, Phys. Rev. Lett. **126**, 106804 (2021).

[51] D. Unuchek, A. Ciarrocchi, A. Avsar, K. Watanabe, T. Taniguchi, and A. Kis, Nature (London) **560**, 340 (2018).

[52] F. A. Rasmussen and K. S. Thygesen, J. Phys. Chem. C **119**, 13169 (2015).

[53] T. Woźniak, P. E. Faria Junior, G. Seifert, A. Chaves, and J. Kunstmann, Phys. Rev. B **101**, 235408 (2020).

[54] D. Xiao, G.-B. Liu, W. Feng, X. Xu, and W. Yao, Phys. Rev. Lett. **108**, 196802 (2012).

[55] F. Katsch, M. Selig, and A. Knorr, Phys. Rev. Lett. **124**, 257402 (2020).

[56] M. S. Hybertsen and S. G. Louie, Phys. Rev. Lett. **55**, 1418 (1985).

[57] R. Geick, C. H. Perry, and G. Rupprecht, Phys. Rev. **146**, 543 (1966).

[58] V. May, F. Boldt, and K. Henneberger, Phys. Status Solidi B **129**, 717 (1985).

[59] F. Boldt, K. Henneberger, and V. May, Phys. Status Solidi B **130**, 675 (1985).

[60] G. Röpke, T. Seifert, and K. Kilimann, Ann. Phys. **493**, 381 (1981).